Friction
https://doi.org/10.1007/s40544-023-0829-4
ISSN 2223-7690
CN 10-1237/TH
RESEARCH ARTICLE

Blackening failure of poly-α-olefin impregnated porous polymide due to the splitting of lubrication oil catalyzed by iron

Pengfei SHI[1], Yang YIN[1], Shaohua ZHANG[2], Diankai ZHANG[1], Yuanyuan JIANG[1], Yang WANG[1], Ningning ZHOU[2], Tao QING[2], Jintao WU[2], Linmao QIAN[1], Jiyang ZHANG[2,*], Lei CHEN[1,3,*]

[1] *Tribology Research Institute, State Key Laboratory of Rail Transit Vehicle System, The School of Mechanical Engineering, Southwest Jiaotong University, Chengdu 610031, China*

[2] *Beijing Key Laboratory of Long-life Technology of Precise Rotation and Transmission Mechanisms, Beijing Institute of Control Engineering, Beijing 100094, China*

[3] *Technology and Equipment of Rail Transit Operation and Maintenance Key Laboratory of Sichuan Province, School of Mechanical Engineering, Southwest Jiaotong University, Chengdu 610031, PR China*

Received: 31 January 2023 / Revised: 10 April 2023 / Accepted: 20 September 2023

Abstract: Lubrication failure accompanying with blackening phenomenon significantly reduces the long-running operational reliability of porous polymide (PPI) lubricated with poly-α-olefin (PAO) oil. Here, the effects of lubrication condition and counter-surface chemistry on the blackening failure of PAO impregnated PPI were studied through the comparison of the tribological tests against GCr15 steel ball and Al_2O_3 ceramic ball with and without PAO oil lubrication. Black products were found to be formed on the PAO impregnated PPI surface slid against steel ball or Al_2O_3 ball added with iron nano-particles, but be absent under the conditions without iron or PAO oil. Further analysis indicated that the iron-catalyzed splitting of PAO oil into small molecule alkanes and following the formation of black organic matter should be mainly responsible for the blackening phenomenon. Molecular dynamic (MD) simulations demonstrated that the iron facilitated the separation of hydrogen atom and the following broken of C–C bonds in PAO molecules, final resulting in the splitting of PAO oil.

Keywords: porous polyimide; poly-α-olefin oil; friction-induced blackening phenomenon; tribological performance; ReaxFF MD simulation

1 Introduction

Owing to its high thermal stability, excellent mechanical properties and self-lubricating performance, porous polyimide (PPI) has been widely adopted in aerospace applications [1–6]. For instance, PPI cage as the key part of aerospace bearing can store and provide lubricating oil meanwhile guiding the movement of bearing rollers, hence the bearing design can be significantly simplified and the weight as well as the cost of spacecraft components can also be largely reduced since the additional oil supply system is no longer needed [7–10].

The superior self-lubricating performance of PPI originates from its uniformly distributed porous structure, which can effectively ensure the suction, storage, and release of lubricating oil [11–13]. During the running stage, the lubricating oil can be released from the porous to form lubrication film in the sliding interface. Previous studies have attempted to facilitate the transference of the stored oil to the outermost contact surfaces through optimizing bulk porosity [14, 15], surface pore size [16] or operating temperature [17, 18]. However, the complex contact feature due to the rough porous PPI surface itself may destroy the stability of lubrication film and result

* Corresponding author: Jiyang ZHANG, E-mail: ziywsy@vip.sina.com; Lei CHEN, E-mail: chenlei@swjtu.edu.cn

in local stress concentration, so the continuous wear of PPI normally accompanying by the generation of black products is still a critical issue to shorten the bearing lifetime [19]. Based on the analyses of the stability, skidding degree, ball–cage collision, wear distribution, and wear rate during the running, Gao et al. [20] indicated that the blackening phenomenon is due to the frequent impulse collisions and wear between the ball and the PPI cage pocket. Jiang et al. [21] studied the tribological behaviors of PPI against a steel ball under a motion compounded with rolling and sliding and found that the rolling–sliding motion facilitated the wear of PPI and the formation of black products. Although the blackening phenomenon has been attracted considerable attentions, its underlying mechanism is far from fully understanding, suppressing the further improvement of tribological performance especially for long-time running of PPI cage.

In this study, the tribological behaviors of PPI slid against GCr15 and Al_2O_3 balls were compared under PAO immersed and un-immersed conditions. Combined with the tests of Al_2O_3 balls slid against PPI after adding iron nano-particles, the key roles of PAO oil and iron element in the blackening phenomenon were detected. More details about the possible tribochemical reactions were deeply discussed based on the further analysis together with molecular dynamic (MD) simulations. The results in this study provide critical insights needed for better understanding of the failure mechanism of polyimide components used in bearings.

2 Material and methods

2.1 Materials

The thermoplastic PPI samples with a porosity of ~20% were used in this study as the friction substrates. Before the friction tests, all PPI surfaces were polished by sandpaper to uniform the root-mean-square surface roughness as 100 ± 5 nm. To simulate the contact condition of PPI cage in bearing, the GCr15 stainless steel and Al_2O_3 ceramics balls with a diameter of 6.35 ± 0.5 mm and a surface roughness of 24 ± 2 nm were chosen as the counterfaces in this study. The PAO oil with a kinematic viscosity of 58.18 mm^2/s at 40 °C purchased from Sinopec Co., Ltd., China was used to immerse PPI. Before each test, the PPI samples and balls were ultrasonically cleaned with absolute alcohol and deionized water for 3 min, following dried in the vacuum drying oven (DZF-6020, Suzhou Sanqing instrument Co., Ltd., China) at 100 °C for 24 hours. Subsequently, the dried PPI samples were immersed in PAO oil for 24 hours to fully infiltrate the internal pores, and then the friction experiments were carried out after wiping off the excess lubricating oil on the outermost surface with a cotton cloth.

2.2 Friction tests and characterizations

The reciprocating sliding friction experiments between PPI samples and balls were carried out by using a high-precision universal tribotester (UMT-TriboLab, Bruker, USA) under room condition (temperature = 23 ± 3 °C; relative humidity = 30 ± 3%), as shown in Fig. 1. The applied load was 5 N, the reciprocating frequency was 10 Hz, the amplitude was 5 mm, and hence the sliding speed was 100 mm/s. All experiments in this study were repeated three times at least. After the tribological tests, all morphologies of the wear tracks were photographed by an optical microscope (Axio Lab.A1, Zeiss, Germany) together with a white light interferometer (WLI, Chotest Superview W1, Chotest Technology Inc., China). The detailed topographies of the PPI cross-sections were imaged using scanning electron microscopy (SEM, Geminisem 300, Zeiss, Germany) and the corresponding changes of chemical components after wear were characterized by using time-of-flight secondary ion mass spectrometry (ToF-SIMS). The component of blackened PAO oils after thermal treatment compared to the pristine sample were studied by gas chromatography and mass spectrometry (GC-MS) method.

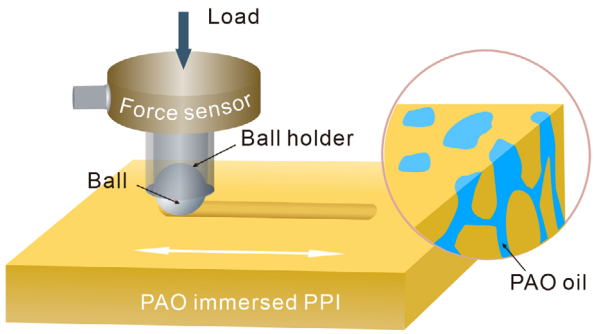

Fig. 1 Schematic illustration showing the friction tests of ball sliding against the PAO oil immersed PPI.

2.3 MD simulations model and details

The MD simulations of PAO-lubricating self-mated iron slabs with the reactive force field (ReaxFF) [22] were conducted to study the reaction mechanism of iron element and PAO oil. Figure 2 shows the friction simulation model where 16 PAO oil molecules were placed between the upper and lower iron slabs. Before friction, the top-layer atoms of the upper iron slab were firstly pressed down with a target pressure of 100 MPa for 50 ps to reach a stable contact state. Then, to conduct friction simulation, the top-layer atoms of the upper iron slab were pressed down with the same normal force and forcibly moved laterally at a velocity of 100 m/s, while the bottom-layer atoms of the lower iron slab were fixed and frozen. In the simulation, velocity-Verlet algorithm [23, 24] was used to evolve atoms with a time step of 0.1 fs under periodic boundary conditions. The system temperature was set to 300 K by the Nose–Hoover chain method [25]. All the snapshots in this paper were generated by the software of OVITO [26].

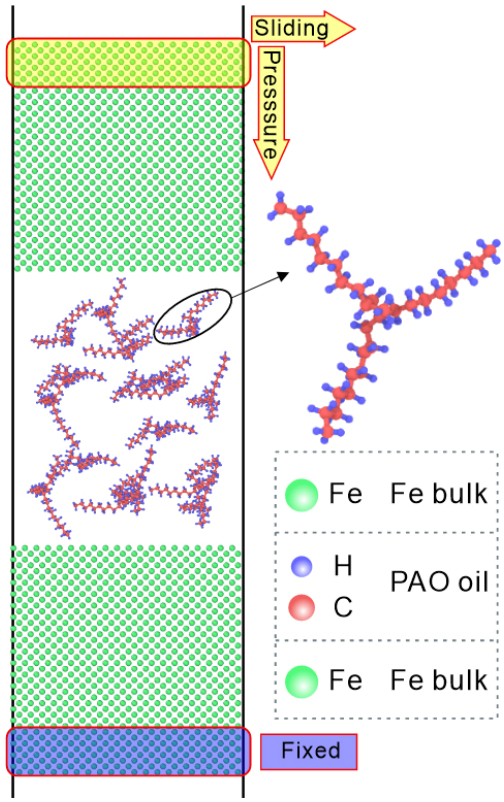

Fig. 2 Simulation model of PAO-lubricating self-mated iron slabs. The iron, hydrogen, and carbon atoms were marked with green, blue and red colors, respectively.

3 Results and discussion

3.1 Tribological behaviors of PPI against GCr15 and Al_2O_3 balls

Here, the tribological behaviors on the PAO immersed PPI surfaces were investigated by using two typical bearing balls, involving GCr15 steel balls and Al_2O_3 ceramic balls. Different friction behaviors were observed for these two balls (Fig. 3(a)). The friction of GCr15/PPI pair increased to a stable coefficient about 0.11 after a short brief drop during the initial 50-s sliding. In comparison, the friction coefficient of Al_2O_3/PPI pair decreased gradually to a steady value around 0.08 after the initial running-in process. The optical images of the worn PPI surfaces show that abound of black products generated in the wear track formed after sliding against GCr15 ball (Fig. 3(b)), whereas no visible color change is observed on the PPI surface after sliding against Al_2O_3 ball (Fig. 3(e)). The WLI three-dimensional topographies and the cross-section profiles of the wear tracks present that surface wear of PPI occur under these two conditions (Figs. 3(c) and 3(f)). In contrast, the wear of GCr15 and Al_2O_3 balls are negligible (Figs. 3(d) and 3(g)). Figure 3(h) compares the friction coefficients averaged after running-in stages and the wear volumes estimated based on the WLI topographies on the two PPI surfaces. The high friction of GCr15/PPI pair corresponds to more severe wear of PPI surface accompanying with blackening phenomenon. For the Al_2O_3/PPI pair, the stable friction is relatively low and no black products formed on the slight worn PPI surface. The results indicate that the steel ball plays a crucial role in the blackening phenomenon on the PPI surface.

3.2 Characterizations of the worn PPI surfaces

The cross-section of the wear regions on the PPI surfaces were imaged using optical microscope and SEM. For the blackening wear track formed after slid against GCr15 ball (Fig. 4(a)), the black products were not only generated on the outermost worn surface, but also diffused into the subsurface with a maximum depth around 300 μm. As a reference, no change in color were observed at the cross-section of the wear track formed after against an Al_2O_3 ball (Fig. 4(e)). Although the different colors were characterized

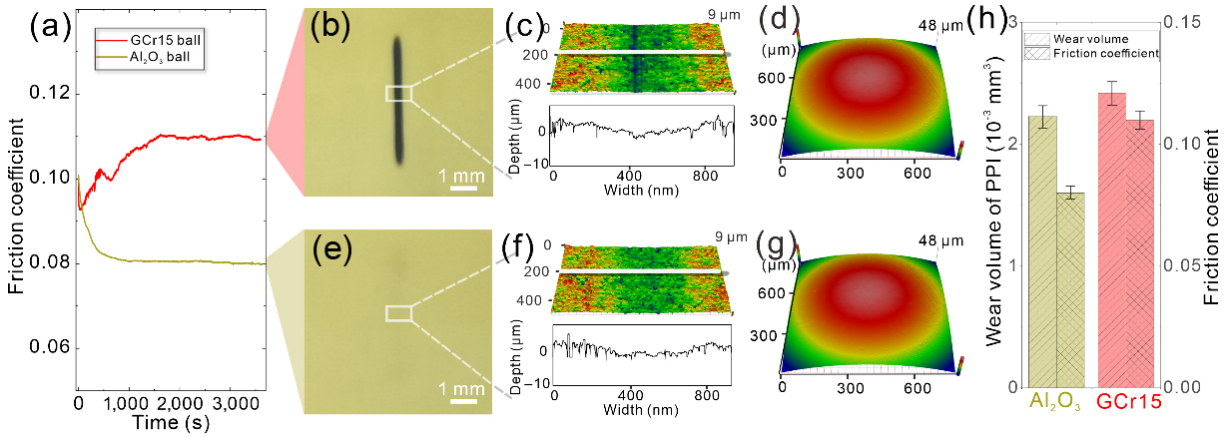

Fig. 3 Friction and wear behaviors of PAO oil immersed PPI slid against GCr15 and Al_2O_3 balls. (a) Friction behaviors of GCr15/PPI and Al_2O_3/PPI pairs under an applied load of 5 N. (b, e) Optical images of the worn PPI surfaces after sliding against these two balls. (c, f) WLI topographies and cross-section profiles of the wear tracks on the PPI surfaces. (d, g) Topographies of the GCr15 and Al_2O_3 balls after the friction tests. (h) Comparison of the wear volumes on PPI surfaces and the stabilized friction coefficients for these two pairs.

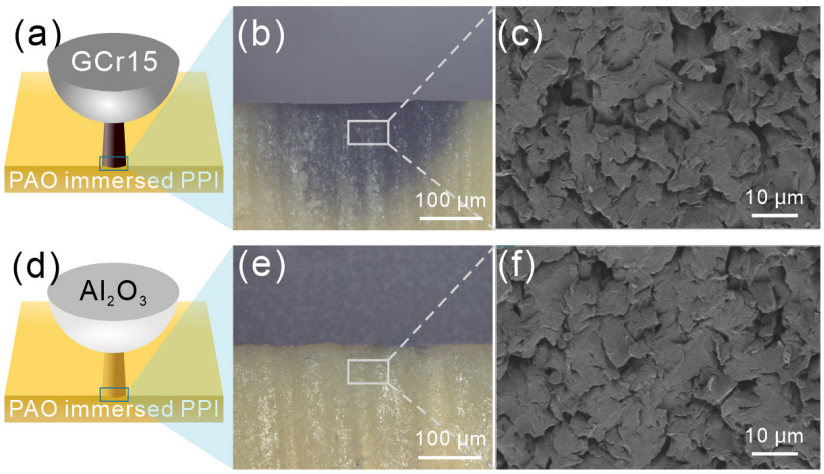

Fig. 4 (b, e) Optical and (c, f) SEM images of the cross-section structure of the wear tracks on PPI surface formed after sliding against (a) GCr15 ball and (b) Al_2O_3 ball, respectively.

in the optical images, the SEM topographies of the cross-sections beneath these two worn tracks are nearly identical (Figs. 4(c) and 4(f)). It supports that the subsurface blackening phenomenon should originate from diffusion rather than inner structure damage of the PPI material.

To further study the possible changes of the PPI materials during the sliding processes, the worn PPI surfaces were characterized by using ToF-SIMS. It was surprising that no significant difference was detected in the wear tracks with and without black products, which were respectively formed after against GCr15 ball (Fig. 5(a)) and Al_2O_3 ball (Fig. 5(b)). The distribution images show the emitted clusters of C_5HNO, $C_6H_7NO_2$, $C_8H_{15}O$, and $C_{10}H_7O$ measured inside these two worn surfaces. All of them belong to PPI material ($C_{23}H_{16}N_4O_5$) and no additional material was observed even in the blackening wear tracks. The ToF-SIMS results indicate that the decomposition of PPI material should have an extreme weak contribution for the black products forming.

Previous study [21] has demonstrated that the PPI is vulnerable to be worn and occur blackening failure under heating condition, so the thermal decomposition of PPI material was proposed as one of the reason for the generation of black products. In this study, no extreme heating was provided and the friction flash temperature at GCr15/PPI sliding interface should be lower than that at Al_2O_3/PPI interface due to the higher thermal conductivity of GCr15 than Al_2O_3. The

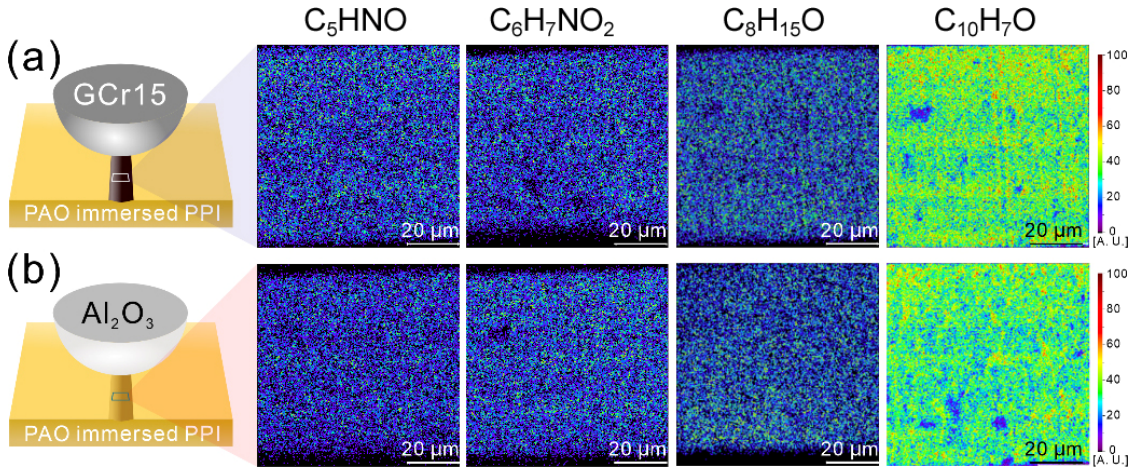

Fig. 5 ToF-SIMS analyses inside the wear tracks with and without black products formed after against (a) GCr15 ball and (b) Al_2O_3 ball, respectively. The distribution images showing the emitted clusters of C_5HNO, $C_6H_7NO_2$, $C_8H_{15}O$, and $C_{10}H_7O$ measured inside the worn regions.

fact combining with the ToF-SIMS results rule out the main contribution of thermal PPI decomposition in the blackening phenomenon. Instead, the roles of steel counterface and PAO oil in these tribochemical reactions should be considered.

3.3 Roles of iron and PAO oil in the blackening phenomenon

To explore the impact of iron element in the frictional blackening behavior, the tribological test of Al_2O_3/PPI pair was conducted with the addition of iron nano-particles with a radius of 200 nm (inset in Fig. 6(a)). Different from the condition without additional particles, the friction increased monotonously from an initial coefficient of ~0.11 (Fig. 6(a)) and the serious blackening failure occurred in the worn region (Fig. 6(b)) when the iron nano-particles were added at the Al_2O_3/PPI interface. The WLI topography and the corresponding cross-section profile (Fig. 6(c)) show severe wear formed on the PPI surface but the damage of the Al_2O_3 ball is still negligible (Figs. 6(d) and 6(e)). The results indicate that the iron nano-particles added at the sliding interface not only caused the scratch wear with high interfacial friction due to plow effect, but also participated in the tribochemical reactions to facilitate the growth of black products.

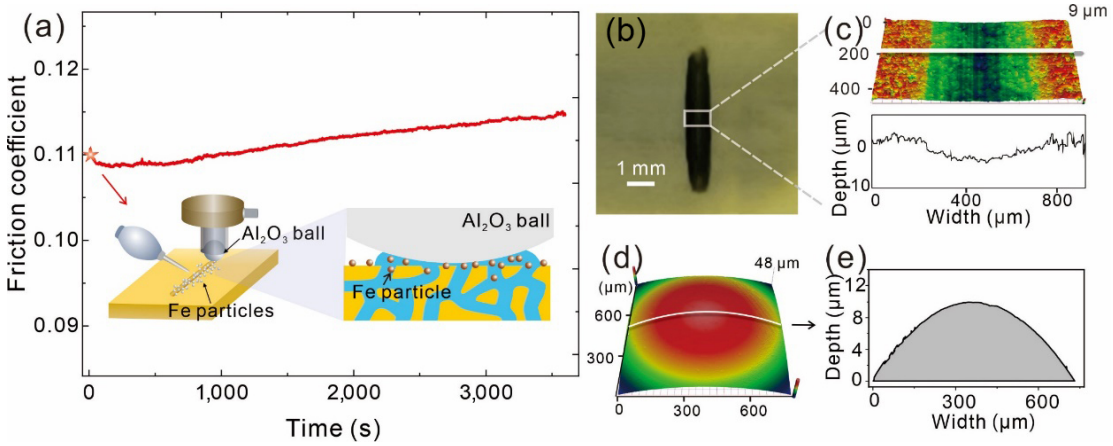

Fig. 6 Tribological behaviors of the Al_2O_3/PPI pair with the addition of iron nano-particles at the sliding interface under PAO oil lubrication. (a) Friction behavior after adding the iron nano-particles. (b, c) Optical image and WLI topography of PPI surface after sliding 1 hour against Al_2O_3 ball with the addition of iron nano-particles. (d, e) WLI topography and the corresponding cross-section profile of the Al_2O_3 ball after the friction test.

The iron oxides are inevitably present on both the surface of the GCr15 steel ball and the added iron particles in Fig. 6, which may also play a role in the frictional blackening behavior. Therefore, the tribological test was conducted between the GCr15/PPI interface with the addition of Fe_2O_3 nano-particles (inset in Fig. 7(a)) to investigate the effect of Fe_2O_3 in the frictional blackening behavior. Contrary to the monotonic increase of the friction coefficient (Fig. 6(a)) with the addition of iron nano-particles, the friction of the Fe_2O_3 nano-particles added has stabilized at ~0.105 (Fig. 7(a)), and only a small amount of red products can be found (may be the Fe_2O_3 clusters) in the worn region (Fig. 7(b)). The WLI topography and the corresponding cross-section profile (Fig. 7(c)) show severe wear formed on the PPI surface but the damage of the Al_2O_3 ball is still negligible (Figs. 7(d) and 7(e)). The results demonstrate that the Fe_2O_3 nano-particles added at the sliding interface did not promote the tribochemical reactions that led to the blackening behavior.

As a comparison, another tribological test of the PPI sample against Al_2O_3 ball was carried out under the condition without PAO oil lubrication (inset in Fig. 8(a)). The dry sliding caused the sharp raise of friction to be a stable coefficient of ~0.28. It is intriguing that no black products can be formed on the worn PPI surface under the condition with additional iron nano-particles but without oil lubrication (Fig. 8(b)) although the severe surface wear formed in the slid region of PPI surface (Fig. 8(c)) and the obvious material removal occurred on the Al_2O_3 ball surface (Figs. 8(d) and 8(e)). High friction should correspond to large frictional flash temperature. The results rule out that the black products originate from the iron oxidations (such as Fe_2O_3 or Fe_3O_4) which should be more likely to happen under the high friction in dry condition. Then, it is reasonable to hypothesize that the blackening phenomenon should be mainly attributed to the degeneration of POA4 oil which can be facilitated by iron element.

3.4 Splitting of PAO oil catalyzed by iron

To detect the role of iron in promoting the oil degeneration, the PAO oil was heated with and without adding an iron plate and further comparatively analyzed by GC-MS method. The pristine PAO oil before thermal treatment is colorless transparent liquid (left inset in Fig. 9(a)). After being heated at 200 °C for 1 hour in the atmospheric environment, the colors of the PAO oil without and with iron plate changed to light yellow (PAO_t, middle inset in Fig. 9(a)) and black ($PAO(Fe)_t$, right inset in Fig. 9(a)), respectively. Subsequently, the above three PAO oils were utilized to lubricate the Al_2O_3/PPI interfaces. The frictions are close for the lubrication with pure PAO oil before and after thermal treatment. The slight degeneration of oil has negligible effect on the lubricating performance. In comparison, the lubrication with the blackened oil increased the friction coefficient to be a

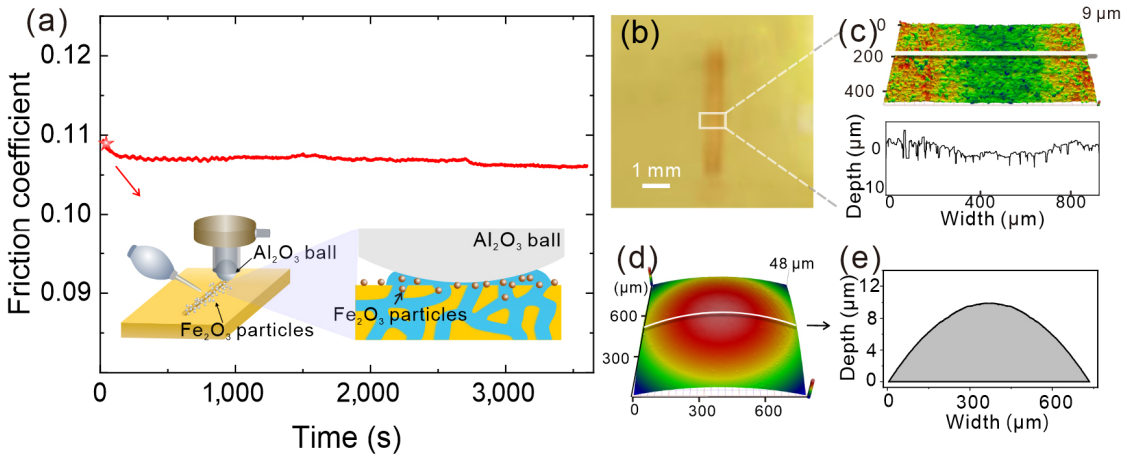

Fig. 7 Tribological behaviors of the Al_2O_3/PPI pair with the addition of Fe_2O_3 nano-particles at the sliding interface under PAO oil lubrication. (a) Friction behavior after adding the Fe_2O_3 nano-particles. (b, c) Optical image and WLI topography of PPI surface after sliding 1 hour against Al_2O_3 ball with the addition of the Fe_2O_3 nano-particles. (d, e) WLI topography and the corresponding cross-section profile of the Al_2O_3 ball after the friction test.

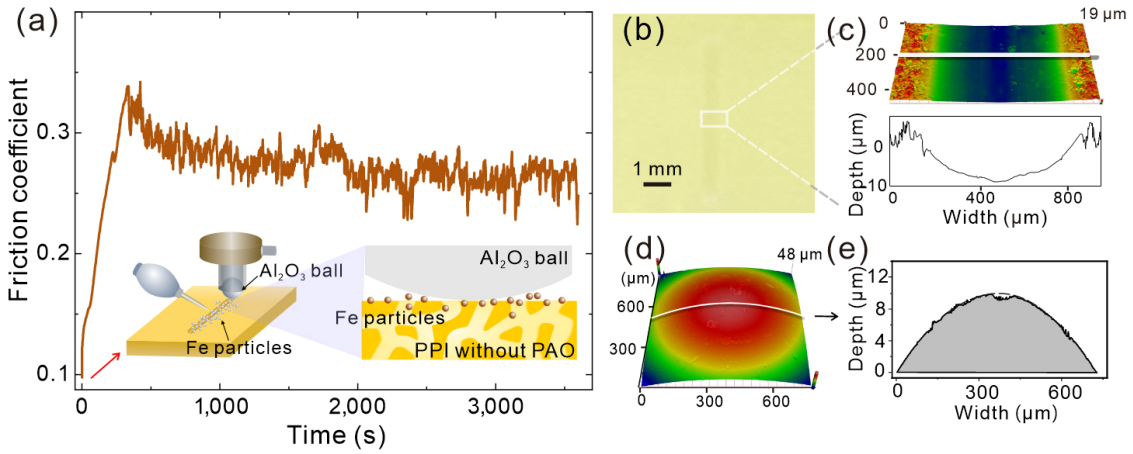

Fig. 8 Tribological behaviors of the Al_2O_3/PPI pair under the conditions with the addition of iron nano-particles but without PAO oil lubrication. (a) Friction behavior under the dry sliding condition. (b, c) Optical image and WLI topography of PPI surface after sliding 1 hour. (d, e) WLI topography and the corresponding cross-section profile of the Al_2O_3 ball after the friction test.

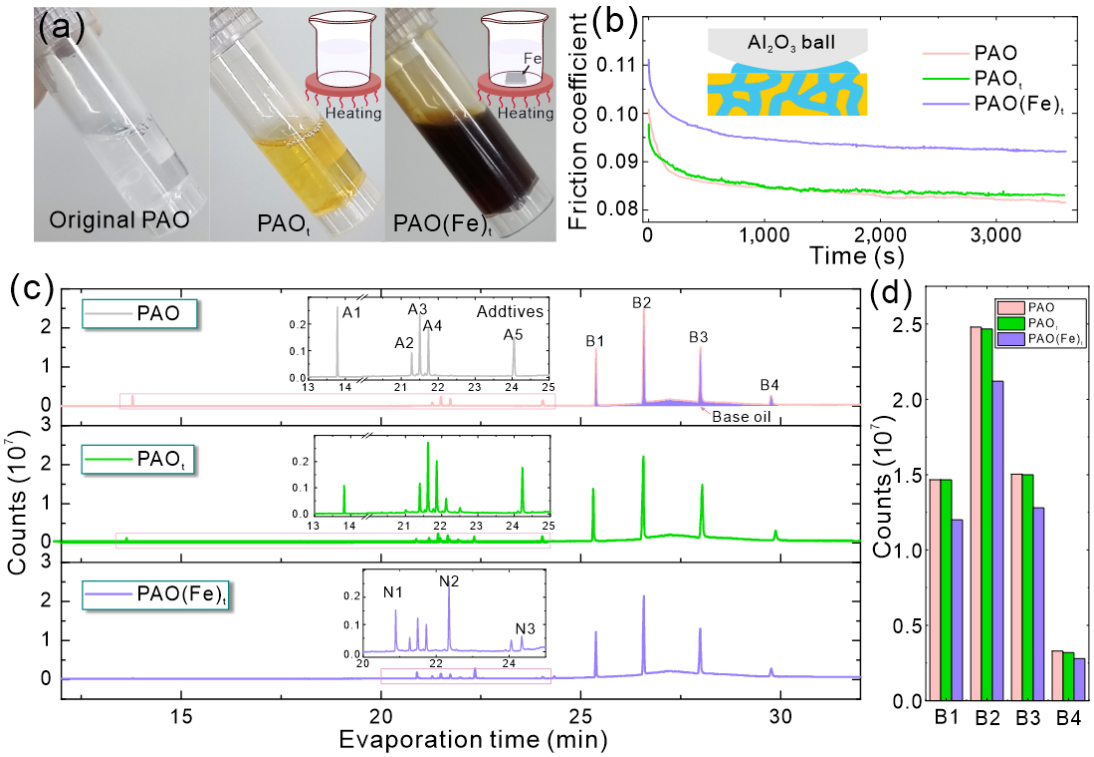

Fig. 9 Characterizations of the PAO oil before and after heated with and without iron plate. (a) Optical images of the pristine PAO oil (PAO), heated PAO oil without (PAO_t) and with iron plate ($PAO(Fe)_t$). (b) Friction behaviors of Al_2O_3/PPI pairs lubricated with PAO, PAO_t and $PAO(Fe)_t$, respectively. (c) Total ion chromatograms of the three PAO oils measured by GC-MS. (d) Maximum counts of the fours peaks (B1–B4) corresponding to the components of base oil.

stable value of 0.095 (Fig. 9(b)). The iron plate facilitated the splitting of the PAO oil, resulting in weak lubricating performance. Figure 9(c) shows the total ion chromatograms of the PAO oil before and after thermal treatments given from GC-MS analysis. All kinds of PAO oil are composed of additives corresponding to the peaks of A1–A5 and base oil corresponding to the peaks of B1–B4 (Fig. 9(c)) [27–29]. The main difference for the blackened oil compared to the other two samples is that there are another three obvious new peaks N1–N3. Furthermore, the max counts of the fours peaks related to the base

oil are close for the pure oil before (PAO) and after (PAO_t) thermal treatment, but reduce significantly for the heated oil with iron plate, $PAO(Fe)_t$ (Fig. 9(d)). The GC-MS results indicate that the iron plate associates the splitting of base oil to generate new compounds, which causes the oil blackening. Further mass spectrums of additives (A1–A5), base oil (B1–B4), and new compounds (N1–N3) illustrate that the new compounds originated from the splitting of base oil (Fig. S1 in Electronic Supplementary Material (ESM)).

MD simulations of PAO-lubricating self-mated iron slabs with ReaxFF [22] were conducted to study the reaction mechanism of iron with PAO oil. Figure 10(a) shows the initial state. Figure 10(b) demonstrates the pressing process of the upper iron slab until all PAO oil molecules are compressed and contacted to the iron slabs (Fig. 10(c)). Figure 10(d) shows the contact interface after sliding 100 ps. MD simulations provide a further insight into the tribochemical reactions at the atomic level. Compared to the contact interface at 12.5 ps (Fig. 10(e)), one H atom (H3) was found to be separated from the C1 carbon atom of PAO molecular and was captured by one Fe atom (Fe4) at 15 ps (Fig. 10(f)) due to the remarkable capacity for hydrogen absorption of iron [30, 31]. Meanwhile, the C1 carbon atom with high chemical activity bonded with the fixed Fe5 iron atom, as shown in Fig. 10(f). Thereafter, the C2 carbon atom moved toward right with the upper slab whereas the C1 carbon atom was pulled by Fe5 fixed iron atom, resulting in the break of C1–C2 bond. The total numbers of C–H and C–C bonds in PAO were shown in Fig. S2 in ESM.

5 Conclusions

The blackening failure of the PAO immersed PPI against the GCr15 steel ball was studied in comparison with the tribological behaviors of Al_2O_3/PPI pair. The blackening phenomenon was found to only occur under the conditions with iron and PAO oil. The degeneration of PPI itself has extreme weak contribution to the blackening phenomenon. Instead, the splitting of PAO oil catalyzed by iron element is responsible for the generation of black products. GC-MS analysis and MD simulations indicate that the iron can facilitate the separation of hydrogen atom from PAO molecules and the following broken of C–C bonds to produce small molecule alkanes.

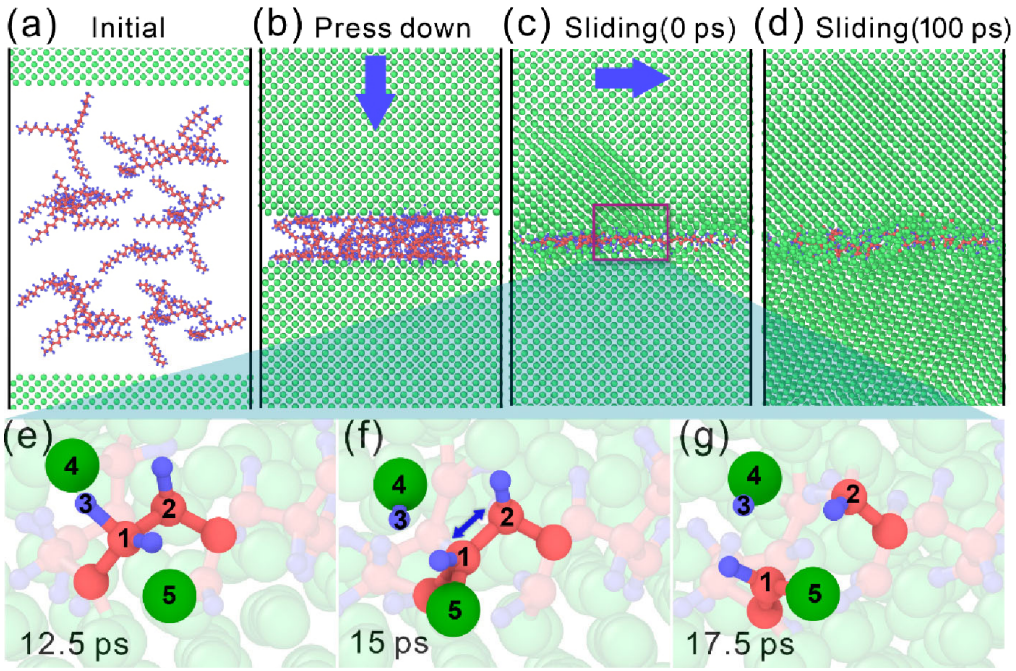

Fig. 10 Tribochemical reactions between iron and PAO molecules in MD simulations, (a–d) showing the snapshots of the pressing and sliding processes. (e–g) Tribochemical reaction process: (e) Initial contact interface of Fe/PAO/Fe; (f) separation of H3 atom from the C1 atom and reacting with iron atom; (g) broken of the C1–C2 bond.

Acknowledgments

This work was supported by the National Natural Science Foundation of China (Nos. 52350411 and 52122507), the National Key Research and Development Program of China (No. 2023YFB3405500), Sichuan Science and Technology Program (Nos. 2023NSFSC1988 and 23NSFTD0030), and the Independent Project of State Key Laboratory of Traction Power (No. 2023TPL-T04). We would like to thank Analytical and Testing Center of Southwest Jiaotong University for the SEM/EDS tests.

Declaration of competing interest

The authors have no competing interests to declare that are relevant to the content of this article. The author Linmao QIAN is the Editorial Board Member of this journal.

Electronic Supplementary Material Supplementary material is available in the online version of this article at https://doi.org/10.1007/s40544-023-0829-4.

References

[1] Wang Q H, Zheng F, Wang T M. Tribological properties of polymers PI, PTFE and PEEK at cryogenic temperature in vacuum. *Cryogenics* **75**: 19–25 (2016)

[2] Lv P X, Dong Z X, Dai X M, Wang H F, Qiu X P. Synthesis and properties of ultralow dielectric porous polyimide films containing adamantane. *J Polym Sci Part A Polym Chem* **56**(5): 549–559 (2018)

[3] Shi Y J, Mu L W, Feng X, Lu X H. The tribological behavior of nanometer and micrometer TiO_2 particle-filled polytetrafluoroethylene/polyimide. *Mater Des* **32**(2): 964–970 (2011)

[4] Lv M, Wang C, Wang Q H, Wang T M, Liang Y M. Highly stable tribological performance and hydrophobicity of porous polyimide material filled with lubricants in a simulated space environment. *RSC Adv* **5**(66): 53543–53549 (2015)

[5] Qi H M, Li G T, Zhang G, Liu G, Yu J X, Zhang L G. Distinct tribological behaviors of polyimide composites when rubbing against various metals. *Tribol Int* **146**: 106254 (2020)

[6] Zhang D, Wang C, Wang Q H, Wang T M. High thermal stability and wear resistance of porous thermosetting heterocyclic polyimide impregnated with silicone oil. *Tribol Int* **140**: 105728 (2019)

[7] Shao M, Li S, Duan C, Yang Z, Qu C, Zhang Y, Zhang D, Wang C, Wang T, Wang Q. Cobweb-like structural stimuli-responsive composite with oil warehouse and transportation system for oil storage and recyclable smart-lubrication. *ACS Appl Mater Interfaces* **10**(48): 41699–41706 (2018)

[8] Yan Z, Jiang D, Gao X M, Zhang C, Hu M, Feng D P, Sun J Y, Weng L J, Wang C. Tribological behavior of WS_2/oil-impregnated porous polyimide solid/liquid composite system. *Ind Lubr Tribol* **71**(3): 459–466 (2019)

[9] Yan Z, Jiang D, Fu Y L, Qiao D, Gao X M, Feng D P, Sun J Y, Weng L J, Wang H Z. Vacuum tribological performance of WS_2–MoS_2 composite film against oil-impregnated porous polyimide: Influence of oil viscosity. *Tribol Lett* **67**(1): 2 (2018)

[10] Wang J Q, Zhao H J, Huang W, Wang X L. Investigation of porous polyimide lubricant retainers to improve the performance of rolling bearings under conditions of starved lubrication. *Wear* **380–381**: 52–58 (2017)

[11] Marchetti M, Meurisse M H, Vergne P, Sicre J, Durand M. Analysis of oil supply phenomena by sintered porous reservoirs. *Tribol Lett* **10**(3): 163–170 (2001)

[12] Bertrand P A, Carré D J. Oil exchange between ball bearings and porous polyimide ball bearing retainers. *Tribol Trans* **40**(2): 294–302 (1997)

[13] Chen W, Wang W, Liang H, Zhu P. Molecular dynamics simulations of lubricant outflow in porous polyimide retainers of bearings. *Langmuir* **37**(30): 9162–9169 (2021)

[14] Xu X, Shu X W, Pei Q, Qin H L, Guo R, Wang X L, Wang Q H. Effects of porosity on the tribological and mechanical

properties of oil-impregnated polyimide. *Tribol Int* **170**: 107502 (2022)

[15] Wang C, Zhang D, Wang Q H, Ruan H W, Wang T M. Effect of porosity on the friction properties of porous polyimide impregnated with poly-α-olefin in different lubrication regimes. *Tribol Lett* **68**(4): 102 (2020)

[16] Ye J Z, Li J B, Qing T, Huang H B, Zhou N N. Effects of surface pore size on the tribological properties of oil-impregnated porous polyimide material. *Wear* **484–485**: 204042 (2021)

[17] Ruan H W, Zhang Y M, Li S, Yang L J, Wang C, Wang T M, Wang Q H. Effect of temperature on the friction and wear performance of porous oil-containing polyimide. *Tribol Int* **157**: 106891 (2021)

[18] Wang J Q, Zhao H J, Huang W, Wang X L. Investigation of porous polyimide lubricant retainers to improve the performance of rolling bearings under conditions of starved lubrication. *Wear* **380–381**: 52–58 (2017)

[19] Sathyan K, Gopinath K, Lee S H, Hsu H Y. Bearing retainer designs and retainer instability failures in spacecraft moving mechanical systems. *Tribol Trans* **55**(4): 503–511 (2012)

[20] Gao S, Han Q K, Zhou N N, Zhang F B, Yang Z H, Chatterton S, Pennacchi P. Dynamic and wear characteristics of self-lubricating bearing cage: Effects of cage pocket shape. *Nonlinear Dyn* **110**(1): 177–200 (2022)

[21] Jiang Y Y, Chen L, Xiao C, Zhou N N, Qing T, Qian L M. Friction and wear behaviors of steel ball against polyimide-PTFE composite under rolling-sliding motion. *Tribol Lett* **69**(3): 100 (2021)

[22] Senftle T P, Hong S, Islam M M, Kylasa S B, Zheng Y X, Shin Y K, Junkermeier C, Engel-Herbert R, Janik M J, Aktulga H M, et al. The ReaxFF reactive force-field: Development, applications and future directions. *NPJ Comput Mater* **2**: 15011 (2016)

[23] Verlet L. Computer "experiments" on classical fluids. I. thermodynamical properties of lennard-jones molecules. *Phys Rev* **159**(1): 98–103 (1967)

[24] Verlet L. Computer "experiments" on classical fluids. II. equilibrium correlation functions. *Phys Rev* **165**(1): 201–214 (1968)

[25] Evans D J, Holian B L. The nose–hoover thermostat. *J Chem Phys* **83**(8): 4069–4074 (1985)

[26] Stukowski A. Visualization and analysis of atomistic simulation data with OVITO-the Open Visualization Tool. *Model Simul Mater Sci Eng* **18**(1): 015012 (2010)

[27] Wu N, Zong Z M, Fei Y W, Ma J, Guo F. Thermal degradation of aviation synthetic lubricating base oil. *Petrol Chem* **58**(3): 250–257 (2018)

[28] Fei Y W, Wu N, Ma J, Hao J T. Thermal cracking of poly α-olefin aviation lubricating base oil. *IOP Conf Ser*: *Earth Environ Sci* **121**: 022031 (2018)

[29] Yosief H O, Sarker M I, Bantchev G B, Dunn R O, Cermak S C. Chemical modification of beef tallow for lubricant application. *Ind Eng Chem Res* **61**(27): 9889–9900 (2022)

[30] Truschner M, Trautmann A, Mori G. The basics of hydrogen uptake in iron and steel. *BHM Berg Und Hüttenmännische Monatsh* **166**(9): 443–449 (2021)

[31] Tanaka H, Ratoi M, Sugimura J. The role of synthetic oils in controlling hydrogen permeation of rolling/sliding contacts. *RSC Adv* **11**(2): 726–738 (2020)

Pengfei SHI. He received his Ph.D. degree in mechanical engineering in 2020 from Southwest Jiaotong University (SWJTU), China. His research interest includes the effect of wear on the performance of transmission components.

Lei CHEN. He is currently a professor of Southwest Jiaotong University (SWJTU), China. He received his Ph.D. degree from SWJTU in 2013 and acted as a visiting scholar in The Pennsylvania State University, USA. His current research interests involve micro/nano-tribology and ultra-precision surface manufacturing.

Jiyang ZHANG. He received his B.S., M.S., and Ph.D. degrees from Beihang University, China, in 1992, 1999, and 2015, respectively. He is currently a senior researcher at Beijing Institute of Control Engineering, China. His research areas cover the spacecraft actuator design and the application of superlubricity.